

# Vector Mapping of Receiver Coordinates to GNSS Time Transfer

Baoying Wei<sup>a</sup>, Kun Liang<sup>a,\*</sup>, Jian Wang<sup>a</sup>, Zhiyu He<sup>b</sup>, Yufeng Li<sup>a</sup>, Junliang Zhao<sup>a</sup>

<sup>a</sup>School of Automation and Intelligence, Beijing Jiaotong University, Beijing 100044, China

<sup>b</sup>China Academy of Railway Sciences Corporation Limited, Beijing 100081, China

\*Corresponding author at: School of Automation and Intelligence, Beijing Jiaotong University, Beijing 100044, China

E-mail address: liangk@bjtu.edu.cn

**Abstract**—*The coordinates of a time transfer station are crucial parameters for time transfer based on Global Navigation Satellite System (GNSS) codes. In dynamic scenarios, larger position errors are introduced, necessitating an analysis and evaluation for the impact of the receiver position error on GNSS time transfer. In this paper, the method for mapping the coordinate vectors of both the receiver and the satellite to GNSS time transfer is proposed. The time transfer error caused by the receiver position error is quantified. The error angle, which can describe the position error of the receiver in three-dimensional space, is defined to characterize the time transfer error along with the position error. An analytical expression describing the relationship between these factors is derived and validated. When the error angle is constant, the time transfer error is approximately linear to the position error. With constant position error, the time transfer error is affected approximately by the cosine function of the error angle.*

**Key words**—*Time transfer error, position error, quantification, linear relationship, cosine relationship, error angle.*

## 1. Introduction

In dynamic scenarios, there are increasing requirements for high-precision time synchronization. For instance, the implementation of Multiple-Input Multiple-Output techniques in 5th Generation Mobile Communication Technology for Railways (5G-R)<sup>[1]</sup> requires that the time difference among system components be less than 65 ns. High-precision time transfer based on Global Navigation Satellite System (GNSS) codes has been extensively developed and widely applied among stationary stations, such as the laboratories contributing to the International Atomic Time (TAI) (see details in [2]-[4]). As the important known parameters, the coordinates of a time transfer station could be accurately calculated beforehand in stationary stations. In mobile stations, it is difficult to fix the position precisely during a short period so the position errors are larger. Therefore, for GNSS time transfer in mobile stations, it is essential to analyze and evaluate the impact of the station position on time transfer.

Various transmission errors may be introduced into GNSS positioning and timing performance during the propagation of GNSS signals, for instance, the tropospheric effects and the ionospheric effects. The tropospheric delay can be represented with the product of the tropospheric refraction in the zenith direction and a mapping function related to the elevation angle<sup>[5]</sup>. Traditional models for zenith tropospheric effect correction include the Saastamoinen model in [6] and the Hopfield model in [7]. Mapping functions such as the Niell Mapping Function in [8], the Vienna Mapping Function 1 in [9], and the Global Mapping Function in [10] are widely used.

Reference [11] demonstrated that reducing the sampling rate of troposphere parameters to 15 minutes and applying constraints in Precise Point Positioning (PPP) time transfer could significantly improve clock solution accuracy, reducing errors by up to a factor of 10 for some stations compared to traditional methods. For the single-frequency users, the ionospheric delay can be corrected by the ionospheric models; for the multi-frequency users, ionospheric effects can be eliminated by forming the linear combination of observations. In Global Positioning System (GPS) single-frequency ionospheric delay correction, the impact of the latitudes and the solar activities on the initial phase and nighttime term of the Klobuchar model were studied in [12]. A ten-parameter Klobuchar-like model was proposed, which could improve ionospheric delay correction by 10% compared to the Klobuchar model. The ionosphere scintillation behavior was studied and modeled in [13]. The effect of the Total Electron Content (TEC) and the Rate of TEC Index on positioning error during solar flares and geomagnetic storms was evaluated in [14]. Reference [15] quantified ionospheric effects on time and frequency transfer solutions. The research showed that the first-order ionospheric delays could reach up to 100 nanoseconds (ns) during ionospheric storms, while the second-order delays were about 8 picoseconds (ps) on quiet days and up to 15 ps during ionospheric storms. These delays could significantly impact the accuracy of time transfer, especially for long-baseline measurements or during periods of high ionospheric activity. The hardware delays in the satellite and the receiver are also among the errors, with the former obtained from the navigation messages and the latter measured and corrected by calibration techniques. A method called Time Differenced Double Difference Carrier Phase (TDDDCP) to estimate differential phase bias or carrier phase bias of NavIC receiver was proposed by [16]. The carrier phase measurements corrected by the TDDDCP method provided better positioning solutions in the Z-coordinate than those from the DDCP method. Precise time transfer can only be achieved with a calibrated receiver. Hardware delay of an uncalibrated receiver will be introduced into the time transfer results, up to a few hundred nanoseconds. The calibration techniques of the receiver are mainly divided into differential calibration<sup>[17]</sup> with an uncertainty about 3.4 ns and absolute calibration<sup>[18]-[22]</sup> with a total uncertainty better than 2 ns. This means that an uncertainty of several nanoseconds will be introduced into the time transfer results.

In [23], the receiver coordinates with errors were mapped by the satellite coordinates to validate the common sense that a 3-meter position error results in a time transfer error of more than 10 ns. However, the analysis relied solely on the geometric distance between the satellite and the receiver, without considering other factors, such as the ionospheric and tropospheric effects. The proposed time transfer error model only considered the geometric distance and did not explain why ionospheric and tropospheric effects are not included. Reference [24] mentioned the phenomenon where the position error led to significant geometric distance error but caused minor errors in the ionospheric delay and the Sagnac effect. Therefore, the conclusion that the position error had little impact on two-way time transfer is inferred in [24]. However, this inference was based on a phenomenon that lacked quantitative description and theoretical analysis and the time transfer error model had not been proposed. The position of the receiver and the satellite in three-dimensional space can be represented by the coordinate vectors, facilitating precise characterization and analysis. To comprehensively analyze the impact, the position error, which can be represented by coordinate vectors of both the receiver and the satellite, should be mapped into GNSS time transfer. This method is defined as the coordinate vector mapping in this paper and is used to study the impact of the position error on time transfer. The coordinate vectors of both the receiver and the satellite will be defined. The effects of the correction terms of the transmission errors in time transfer will be analyzed individually. The combined impact of these effects on time transfer will be studied. After the theoretical analysis, an analytical expression of time transfer error caused by the position error will be proposed in the paper.

## **2. Coordinate vectors and GNSS observation**

A Cartesian coordinate system is defined in this section for describing the coordinate vectors of the receiver and the satellite. Since GNSS time transfer is conducted based on GNSS observation equations, this section will

present the expressions for the observation equations based on the coordinate vectors.

## 2.1. Coordinate vectors of the receiver and the satellite

Position A and position B are defined to represent the true position and the position with an error. A local Cartesian coordinate system (E, N, U) with position A as the origin is constructed as shown in Fig. 1, whose E-axis points to the east and N-axis points to the north.  $\rho_A$  and  $\rho_B$  are the vector from position A to the satellite and the vector from position B to the satellite, respectively.  $r$  is the vector from position A to position B. The module of  $r$  is defined as the position error.  $\Delta E$ ,  $\Delta N$  and  $\Delta U$  are the projection of  $r$  onto the E-axis, the N-axis and the U-axis, respectively, which are defined as the coordinate errors. The relationship between the position error and the coordinate errors is expressed as follows:

$$\|r\| = \sqrt{\Delta E^2 + \Delta N^2 + \Delta U^2} \quad (1)$$

$\theta_{El,A}$  and  $\theta_{Az,A}$  are the elevation and the azimuth of the satellite observed at position A. The angle between  $\rho_A$  and  $r$  is defined as the error angle  $\theta_{EA}$ .

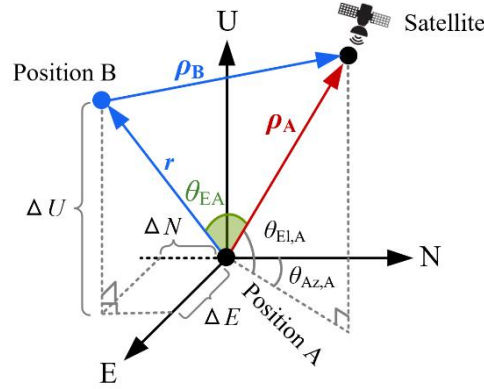


**Fig. 1.** A local Cartesian coordinate system (E, N, U) with position A as the origin.

## 2.2. Relationship between time transfer error and GNSS observation

The pseudorange measurement on single-frequency is used to comprehensively analyze the correction terms of errors in GNSS time transfer including the ionospheric effects.  $T_{L-G}$  is the time difference between the local clock and the GNSS system time (GNSS-T) and can be calculated as (2) and (3), with the principles detailed in [25]. The subscript A/B indicates that this is a variable based on position A/B.

$$T_{L-G,A} = \frac{1}{c} (P_A - \|\rho_A\| - S_A) + T_{rel,A} - T_{tropo,A} - T_{iono,A} - GD_A + T_{sat,A} \quad (2)$$

$$T_{L-G,B} = \frac{1}{c} (P_B - \|\rho_B\| - S_B) + T_{rel,B} - T_{tropo,B} - T_{iono,B} - GD_B + T_{sat,B} \quad (3)$$

$c$  is the velocity of the light.  $P$  is the pseudorange measurement, which has been corrected with the hardware delays of the GNSS time transfer receiver.  $\|\rho_A\|$  and  $\|\rho_B\|$  are the geometric distances from positions A and B to the satellite separately.  $S$  is the Sagnac correction associated with the earth's rotation.  $T_{rel}$  is the relativistic clock correction.  $T_{iono}$  and  $T_{tropo}$  are the ionospheric delay and the tropospheric delay, respectively.

$GD$  is the broadcast group delay.  $T_{\text{sat}}$  is the satellite clock correction.  $S$ ,  $T_{\text{rel}}$ ,  $GD$  and  $T_{\text{sat}}$  which can be calculated by the known parameters and the correction models, such as the rotational speed of the earth, are independent of the receiver coordinates. If the pseudorange measurement  $P_A$  and  $P_B$  at positions A and B are constrained to be equal, the time transfer error  $\Delta T_{L-G}$  caused by the position error can be expressed as follows:

$$\begin{aligned}\Delta T_{L-G} &= T_{L-G,B} - T_{L-G,A} \\ &= \frac{1}{c} (\|\rho_A\| - \|\rho_B\|) + T_{\text{tropo},A} - T_{\text{tropo},B} + T_{\text{iono},A} - T_{\text{iono},B}\end{aligned}\quad (4)$$

### 3. Coordinate vectors mapping to GNSS time transfer

From (4) in section 2.2, it can be seen that the time transfer error is affected by the geometric distance, the ionospheric delay, and the tropospheric delay. The impact of the position error on the three types of delay will be analyzed in sections 3.1 to 3.3. In section 3.4, the combined impact on GNSS time transfer will be studied.

#### 3.1. Geometric distance delay

The geometric distance between the satellite and the receiver causes signal propagation delay, defined as the geometric distance delay. The impact of the position error on the geometric distance delay will be analyzed through theoretical analysis and data fitting.  $\Delta T_{\text{geo}}$  is the error of the geometric distance delay caused by the position error, and it can be calculated as follows:

$$\begin{aligned}\Delta T_{\text{geo}} &= \frac{\|\rho_A\| - \|\rho_B\|}{c} \\ &= \frac{\|\rho_A\| - \sqrt{\|\mathbf{r}\|^2 + \|\rho_A\|^2 - 2\|\mathbf{r}\|\|\rho_A\|\cos\theta_{EA}}}{c}\end{aligned}\quad (5)$$

$\|\mathbf{r}\|$  and  $\theta_{EA}$  are both independent variables of  $\Delta T_{\text{geo}}$ . Equations (6) and (7) are the first and the second order derivative functions of  $\Delta T_{\text{geo}}$  with respect to  $\|\mathbf{r}\|$ , respectively.

$$\left[ \Delta T_{\text{geo}} \right]'_{\|\mathbf{r}\|} = - \frac{\|\mathbf{r}\| - \|\rho_A\| \cos\theta_{EA}}{c \sqrt{\|\mathbf{r}\|^2 + \|\rho_A\|^2 - 2\|\mathbf{r}\|\|\rho_A\|\cos\theta_{EA}}}\quad (6)$$

$$\left[ \Delta T_{\text{geo}} \right]''_{\|\mathbf{r}\|} = \frac{\|\rho_A\|^2 (\cos^2\theta_{EA} - 1)}{c \left( \|\mathbf{r}\|^2 + \|\rho_A\|^2 - 2\|\mathbf{r}\|\|\rho_A\|\cos\theta_{EA} \right)^{1.5}}\quad (7)$$

To make the analysis more realistic, the maximum position error of 5000 meters (m), which is the worst case of the international Search and Rescue services<sup>[26]</sup> for the Beidou Navigation Satellite System (BDS), is taken as an example. The maximum value of  $\|\mathbf{r}\|$  is set to 5000 m.  $\theta_{EA}$  varies from  $0^\circ$  to  $180^\circ$ . In light of the fact that  $\|\mathbf{r}\|$  is much smaller than  $\|\rho_A\|$  by tens of thousands of kilometers (km), the value of  $\left[ \Delta T_{\text{geo}} \right]''_{\|\mathbf{r}\|}$  can be estimated.

When  $\theta_{EA}$  is  $0^\circ$  or  $180^\circ$ ,  $[\Delta T_{geo}]''_{\|r\|}$  reaches the maximum value of 0; when  $\theta_{EA}$  is  $90^\circ$ ,  $[\Delta T_{geo}]''_{\|r\|}$  reaches the minimum value of  $-\|\rho_A\|^2 / [c(\|r\|^2 + \|\rho_A\|^2)^{1.5}]$ , which approximates to 0. It can be deduced that  $[\Delta T_{geo}]'_{\|r\|}$  can be regarded as a constant. Therefore, an approximately linear relationship between  $\|r\|$  and  $\Delta T_{geo}$  can be inferred and expressed as (8).  $k$  is the proportional factor and depends only on  $\theta_{EA}$  and  $\|r\|$ . When  $\theta_{EA}$  is  $0^\circ$ ,  $k$  reaches its maximum value of  $1/c$ ; when  $\theta_{EA}$  is  $90^\circ$  or  $180^\circ$ ,  $k$  reaches its minimum value of  $-1/c$ .

$$\begin{cases} \Delta T_{geo} = k \|r\| \\ k = [\Delta T_{geo}]'_{\|r\|} = -\frac{\|r\| - \|\rho_A\| \cos \theta_{EA}}{c \sqrt{\|r\|^2 + \|\rho_A\|^2 - 2\|r\| \|\rho_A\| \cos \theta_{EA}}} \end{cases} \quad (8)$$

A satellite with a lower orbital altitude exhibits a larger difference between  $\|\rho_A\|$  and  $\|\rho_B\|$  for the same  $\|r\|$ , which results in a larger  $\Delta T_{geo}$ . Therefore, the BDS Medium Earth Orbit (MEO) satellite with an orbital altitude of 21528 km is selected for  $\Delta T_{geo}$  calculation. Based on the geometric relationship shown in Fig. 1, the corresponding values of  $\Delta T_{geo}$  to different values of  $\|r\|$  and  $\theta_{EA}$  can be calculated, which are the black hollow dots shown in Fig. 2. The linear function  $y_{\theta_{EA}}$  is used to fit the values of  $\Delta T_{geo}$  when  $\theta_{EA}$  are  $0^\circ$ ,  $45^\circ$ ,  $90^\circ$ ,  $135^\circ$ , and  $180^\circ$ , respectively. By adjusting the proportional factor of the linear function, the fitting of  $\Delta T_{geo}$  can be achieved. The conclusion inferred from the good fit phenomenon is that when  $\theta_{EA}$  is constant, the relationship between  $\|r\|$  and  $\Delta T_{geo}$  can be approximated as a linear relationship.

$\theta_{EA}$  influences  $\Delta T_{geo}$ , in conjunction with  $\|r\|$ . Thus, it is necessary to analyze the relationship between  $\Delta T_{geo}$  and  $\theta_{EA}$ . The relationship between them can be approximated by data fitting. In Fig. 3, in the cases of different constant values of  $\|r\|$ , the values of  $\Delta T_{geo}$  can be fitted by different cosine functions with different values of amplitude. Therefore, when  $\|r\|$  is held constant, the relationship between  $\Delta T_{geo}$  and  $\theta_{EA}$  can be approximated by a cosine function, as expressed in (9).  $A$  is the amplitude of the cosine function.

$$\Delta T_{geo} = A \cos \theta_{EA} \quad (9)$$

In the case where  $\|r\|$  is 5000 m and  $\|\rho_A\|$  is 21528 km, the maximum of  $\Delta T_{geo}$  is 16678.2 ns and the minimum is 1.9 ns. For the more common case where  $\|r\|$  is 5 m, the maximum and minimum values of  $\Delta T_{geo}$

are 16.7 ns and  $1.5 \times 10^{-6}$  ns, respectively.

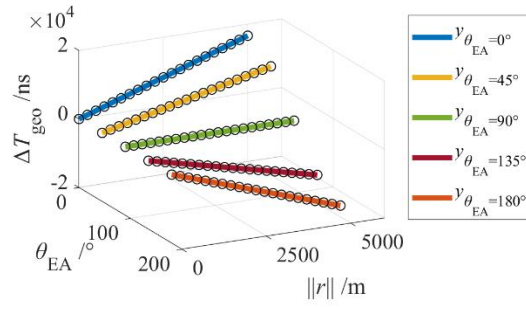


**Fig. 2.** The values of  $\Delta T_{\text{geo}}$  correspond to different values of  $\|r\|$  and  $\theta_{\text{EA}}$ . The functions used for fitting are:

$$y_{\theta_{\text{EA}}=0^\circ} = 3.34\|r\|, \quad y_{\theta_{\text{EA}}=45^\circ} = 2.36\|r\|, \quad y_{\theta_{\text{EA}}=90^\circ} = 0\|r\|, \quad y_{\theta_{\text{EA}}=135^\circ} = -2.36\|r\|, \quad y_{\theta_{\text{EA}}=180^\circ} = -3.34\|r\|.$$

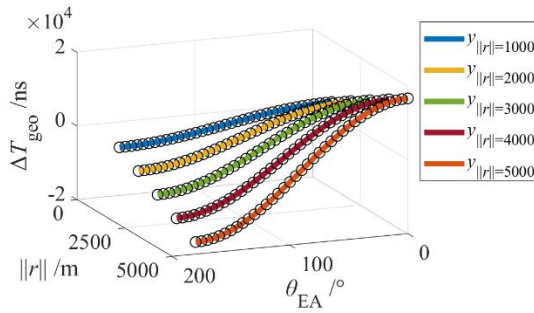


**Fig. 3.** The values of  $\Delta T_{\text{geo}}$  correspond to different values of  $\|r\|$  and  $\theta_{\text{EA}}$ . The functions used for fitting are:

$$y_{\|r\|=1000} = 3340\cos(\theta_{\text{EA}}), \quad y_{\|r\|=2000} = 6670\cos(\theta_{\text{EA}}), \quad y_{\|r\|=3000} = 10000\cos(\theta_{\text{EA}}), \quad y_{\|r\|=4000} = 13300\cos(\theta_{\text{EA}}),$$

$$y_{\|r\|=5000} = 16700\cos(\theta_{\text{EA}}).$$

### 3.2. Tropospheric delay

The tropospheric delay  $T_{\text{tropo,A}}$  at position A, computed by the standard North Atlantic Treaty Organization (NATO) hydrostatic model, is calculated following the procedure shown in Fig. 4.  $f(\theta_{\text{El,A}})$  is a tropospheric mapping function of the elevation  $\theta_{\text{El,A}}$ .  $\Delta R(h_A)$  is the total tropospheric delay at the zenith for the ellipsoidal height  $h_A$  of position A.

**Total tropospheric delay at the zenith**

$$R(h_A) = \begin{cases} \frac{1}{c} \left[ 2162 + 324.8(1-h_A) - 22.3449(1-h_A^2) \right] 10^{-3}, h_A \leq 1 \\ \frac{1}{c} \left[ 732 - 2283.8174 \left( 0.3749 - e^{0.1227(1-h_A)} \right) \right] 10^{-3}, h_A > 1 \end{cases}$$

**Mapping function**

$$f(\theta_{El,A}) = \left( \sin \theta_{El,A} + \frac{0.00143}{\tan \theta_{El,A} + 0.0455} \right)^{-1}$$

**Tropospheric delay**

$$T_{\text{tropo},A} = f(\theta_{El,A}) R(h_A)$$

**Fig. 4.** The calculation process of the tropospheric delay  $T_{\text{tropo},A}$  at position A.

$\theta_{El,B}$  and  $h_B$  are the elevation of the satellite observed at position B and the ellipsoidal height of position B, respectively. The NATO hydrostatic model is used for the computation of the tropospheric delay  $T_{\text{tropo},B}$  at position B.  $f(\theta_{El,B})$  is the tropospheric mapping function of  $\theta_{El,B}$ .  $\Delta R(h_B)$  is the total tropospheric delay at the zenith for  $h_B$ . The tropospheric delay error  $\Delta T_{\text{tropo}}$  caused by the position error can be calculated as follows:

$$\begin{aligned} \Delta T_{\text{tropo}} &= T_{\text{tropo},B} - T_{\text{tropo},A} \\ &= f(\theta_{El,B}) R(h_B) - f(\theta_{El,A}) R(h_A) \end{aligned} \quad (10)$$

The impact of the position error  $\|\mathbf{r}\|$  on the tropospheric mapping function is analyzed first. The position error sphere with radius  $\|\mathbf{r}\|$ , is shown in Fig. 5. The angle between  $\boldsymbol{\rho}_A$  and  $\boldsymbol{\rho}_B$  is defined as  $\omega$ . When the line defined by  $\boldsymbol{\rho}_B$  is tangent to the position error sphere,  $\omega$  reaches the maximum value, denoted as  $\omega_{\max}$ , which is expressed as

$$\omega_{\max} = \arcsin \left( \frac{\|\mathbf{r}\|}{\|\boldsymbol{\rho}_A\|} \right) \quad (11)$$

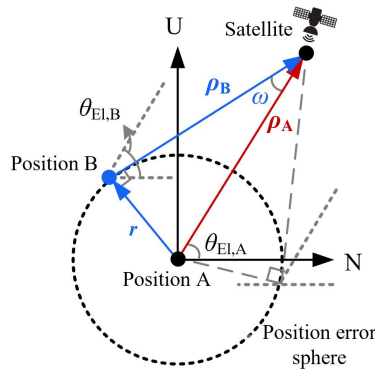


**Fig. 5.** Diagram of the position error sphere.

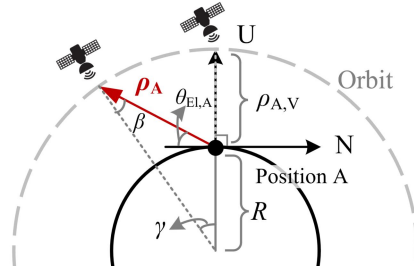


**Fig. 6.** Different values of elevation  $\theta_{El,A}$  result in different values of  $\|\rho_A\|$ .

In order to estimate the range of  $\theta_{El,B}$ , only the maximum value  $\omega_{max}$  of  $\omega$  is considered. As shown in Fig. 6, different values of  $\theta_{El,A}$  result in different values of  $\|\rho_A\|$ . The earth is considered as a sphere with the earth's mean spherical radius  $R$ .  $\rho_{A,V}$  is the geometric distance between the satellite and position A when the satellite over position A.  $\gamma$  is an angle defined for auxiliary calculation.  $\|\rho_A\|$  can be treated as a dependent variable of  $\theta_{El,A}$  and expressed as follows:

$$\|\rho_A\| = \frac{(\rho_{A,V} + R)\sin\gamma}{\sin(\theta_{El,A} + 90^\circ)} \quad (12)$$

$$\gamma = 90^\circ - \theta_{El,A} - \beta \quad (13)$$

$$\beta = \arcsin\left(\frac{R\sin(\theta_{El,A} + 90^\circ)}{(\rho_{A,V} + R)}\right) \quad (14)$$

$\|r\|$  is set to 5000 m. In order to maximize  $\omega_{max}$ ,  $\rho_{A,V}$  is set to 21528 km, which is the altitude of the BDS MEO satellite. The corresponding values of  $\omega_{max}$  to different values of  $\theta_{El,A}$  are shown in Fig. 7. Since  $\sin(\theta_{El,A} + 90^\circ)$ , which is the denominator of (12), cannot be 0, the value of  $\omega_{max}$  when  $\theta_{El,A}$  of  $90^\circ$  is not calculated. The phenomenon that the higher  $\theta_{El,A}$  leads to the larger  $\omega_{max}$  is demonstrated in Fig. 7. With a difference of no more than  $0.003^\circ$  between the maximum and minimum values of  $\omega_{max}$ ,  $\omega_{max}$  takes the maximum value of  $0.0133^\circ$  in the subsequent analysis, regardless of the different values of  $\theta_{El,A}$ . Therefore, when the position error is 5000 m,  $\theta_{El,B}$  is within the interval  $[\theta_{El,A} - 0.0133^\circ, \theta_{El,A} + 0.0133^\circ]$ . Fig. 8 shows  $f(\theta_{El,A})$  for varying  $\theta_{El,A}$ . As  $\theta_{El,A}$  increases, both the rate of change and the value of  $f(\theta_{El,A})$  decrease. This relationship also holds between  $\theta_{El,B}$  and  $f(\theta_{El,B})$ . As the midpoint of the interval for  $\theta_{El,B}$ , a lower  $\theta_{El,A}$  results in a larger difference between  $f(\theta_{El,A})$  and  $f(\theta_{El,B})$ , which may lead to a larger  $\Delta T_{tropo}$ .

according to (10). Since  $(\theta_{\text{El,A}} - 0.0133^\circ)$  becomes negative when  $\theta_{\text{El,A}}$  is smaller than  $0.0133^\circ$ ,  $\theta_{\text{El,A}}$  is taken as  $0.0133^\circ$ .

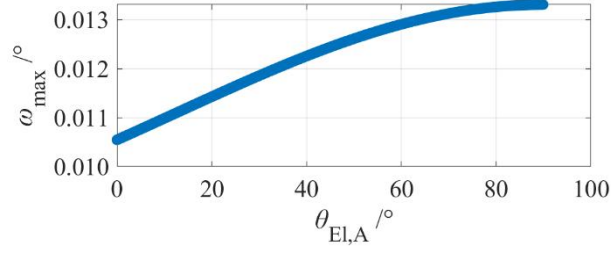


**Fig. 7.** The values of  $\omega_{\text{max}}$  correspond to different values of  $\theta_{\text{El,A}}$ .

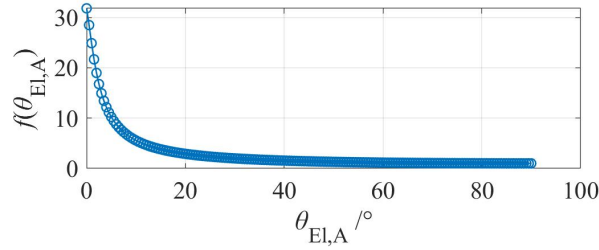


**Fig. 8.** The values of  $f(\theta_{\text{El,A}})$  correspond to different values of  $\theta_{\text{El,A}}$ .

The impact of the position error on the total tropospheric delay at the zenith is analyzed secondly. The values of  $R(h_A)$  corresponding to  $h_A$  from -5000 m to 5000 m are shown in Fig. 9. The portion of the parabola  $y(h_T)$  to the left of the vertex can be used to fit  $R(h_A)$ , which means that both the rate of change and the value of  $R(h_A)$  decrease as  $h_A$  increases. A smaller  $h_A$ , combined with a larger difference between  $h_A$  and  $h_B$ , will result in a larger  $\Delta T_{\text{tropo}}$ . Since the earth is modeled as a sphere, the difference between  $h_A$  and  $h_B$  is considered as the projection of  $\mathbf{r}$  on the U-axis. It can be inferred that  $\Delta U$  should be as large as possible to obtain a larger  $\Delta T_{\text{tropo}}$ .

A special case is set to find the maximum of  $\Delta T_{\text{tropo}}$ , where  $h_A$  is 0 m,  $\theta_{\text{El,A}}$  is  $0^\circ$ ,  $\|\mathbf{r}\|$  is 5000 m,  $h_E$  is -5000 m. In this case, even though the actual value of  $\omega_{\text{max}}$  is less than  $0.0133^\circ$ , it is set to  $0.0133^\circ$  to maximize the difference between  $f(\theta_{\text{El,A}})$  and  $f(\theta_{\text{El,B}})$ . Then  $\Delta T_{\text{tropo}}$  is calculated to be 230.6 ns. That is, a position error of 5000 m will result in a maximum tropospheric delay error of 230.6 ns. In the case where  $\|\mathbf{r}\|$  is 5 m,  $h_B$  is -5000 m,  $h_A$  is -4995 m, the maximum tropospheric delay error is 0.3 ns.

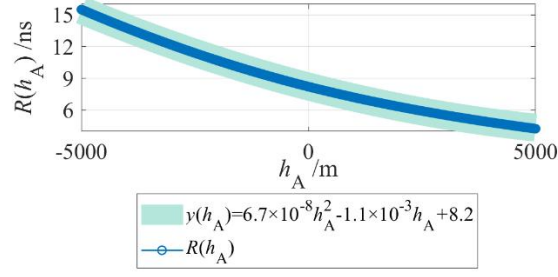


**Fig. 9.** The values of  $\Delta R(h_A)$  correspond to different values of  $h_A$ .

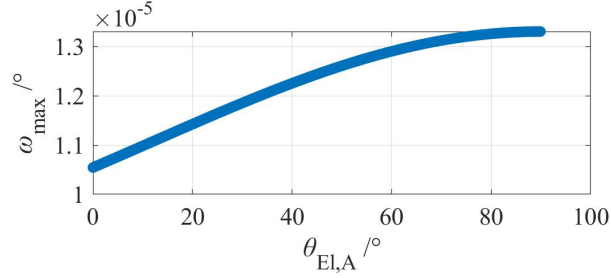


**Fig. 10.** The values of  $\omega_{\max}$  correspond to different values of  $\theta_{El,A}$  when  $\|r\|$  is 5 m.

### 3.3. Ionospheric delay

The calculation process of ionospheric delay  $T_{iono,A}$  at position A based on the Klobuchar model is shown in Fig. 11. The vertical ionospheric delay  $T_{iono,V,A}$  is fitted by a positive half cosine function of  $t_A$ , which is the local time at the Ionospheric Pierce Point (IPP).  $AMP$  and  $PER$  are the amplitude and the period of the positive half cosine function.  $\varphi_{m,A}$  is the geomagnetic latitude of IPP, which can be calculated by the latitude, the longitude,  $\theta_{Az,A}$  and  $\theta_{El,A}$ .  $\alpha_i$  and  $\beta_i$  are the ionospheric parameters obtained from the GNSS navigation message. The ionospheric delay  $T_{iono,A}$  at position A can be converted from  $T_{iono,V,A}$  with an ionospheric mapping function  $F(\theta_{El,A})$ .

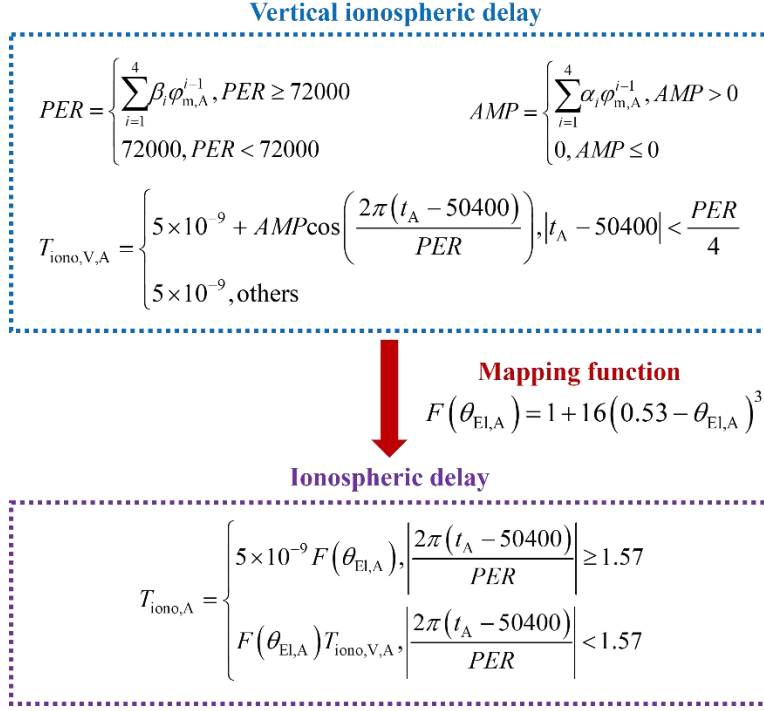


**Fig. 11.** The calculation process of the ionospheric delay  $T_{\text{iono},A}$  at position A.

The ionospheric delay error  $\Delta T_{\text{iono}}$  caused by the position error can be expressed as follows:

$$\begin{aligned} \Delta T_{\text{iono}} &= T_{\text{iono},B} - T_{\text{iono},A} \\ &= \begin{cases} 5 \times 10^{-9} (F(\theta_{\text{El},B}) - F(\theta_{\text{El},A})), & \left| \frac{2\pi(t_{A/B} - 50400)}{PER} \right| \geq 1.57 \\ F(\theta_{\text{El},B}) T_{\text{iono},V,B} - F(\theta_{\text{El},A}) T_{\text{iono},V,A}, & \left| \frac{2\pi(t_{A/B} - 50400)}{PER} \right| < 1.57 \end{cases} \end{aligned} \quad (15)$$

$T_{\text{iono},B}$  is the ionospheric delay at position B calculated by the Klobuchar model.  $T_{\text{iono},V,B}$  and  $\theta_{\text{El},B}$  are the vertical ionospheric delay and the elevation of position B, respectively. The subscript A/B indicates that both  $t_A$  and  $t_B$  satisfy the same condition. In the case of  $\left| \frac{2\pi(t_{A/B} - 50400)}{PER} \right| \geq 1.57$ , that is, during the nighttime,  $\Delta T_{\text{iono}}$  depends only on  $\theta_{\text{El},A}$  and  $\theta_{\text{El},B}$ . Fig. 12 shows the values of  $F(\theta_{\text{El},A})$  correspond to different values of  $\theta_{\text{El},A}$ . As  $\theta_{\text{El},A}$  increases, both the rate of change and the value of  $f(\theta_{\text{El},A})$  decrease.  $\omega_{\text{max}}$  caused by the position error  $\|\mathbf{r}\|$  has been calculated in section 3.2. Therefore, the maximum absolute value of  $\Delta T_{\text{iono}}$  during the nighttime can be calculated based on  $F(\theta_{\text{El},T} = 0^\circ)$  and  $F(\theta_{\text{El},E} = \omega_{\text{max}})$ , which are  $5.0 \times 10^{-3}$  ns when  $\|\mathbf{r}\|$  is 5000 m and  $5.0 \times 10^{-6}$  ns when  $\|\mathbf{r}\|$  is 5 m.

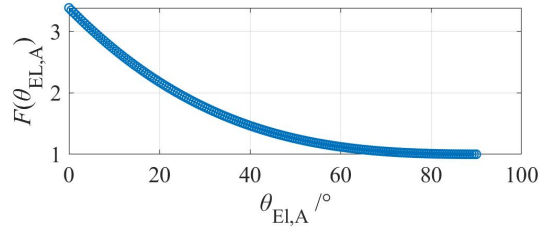


**Fig. 12.** The values of  $F(\theta_{EI,A})$  correspond to different values of  $\theta_{EI,A}$ .

In the case of  $|2\pi(t_{A/B} - 50400) / PER| < 1.57$ ,  $T_{iono,V,A}$  is determined by the geographic longitude, the latitude,  $\theta_{Az,A}$ ,  $\theta_{EI,A}$  and  $t_A$ . Since there are too many parameters that need to be analyzed,  $T_{iono,V,A}$  will be calculated by traversing parameters to find those that lead to the fastest rate of change in the vertical ionospheric delay.  $t_A$  is determined by the GNSS signal transmission time and the position of IPP. Since  $T_{iono,V,A}$  is calculated by traversing the parameters including  $t_A$ , the GNSS signal transmission time can be taken as any epoch within a GPS week.  $\theta_{EI,A}$  is taken as  $0^\circ$  to ensure that  $F(\theta_{EI,A})$  achieves both its maximum value and rate of change, providing  $T_{iono,A}$  with the opportunity to reach its maximum. The ionospheric parameters are derived from the broadcast ephemeris on September 5, 2023. The corresponding values of  $T_{iono,V,A}$  to different values of latitude (only the northern hemisphere is considered), longitude, and  $\theta_{Az,A}$  are shown from Fig. 13(a) to 13(e).

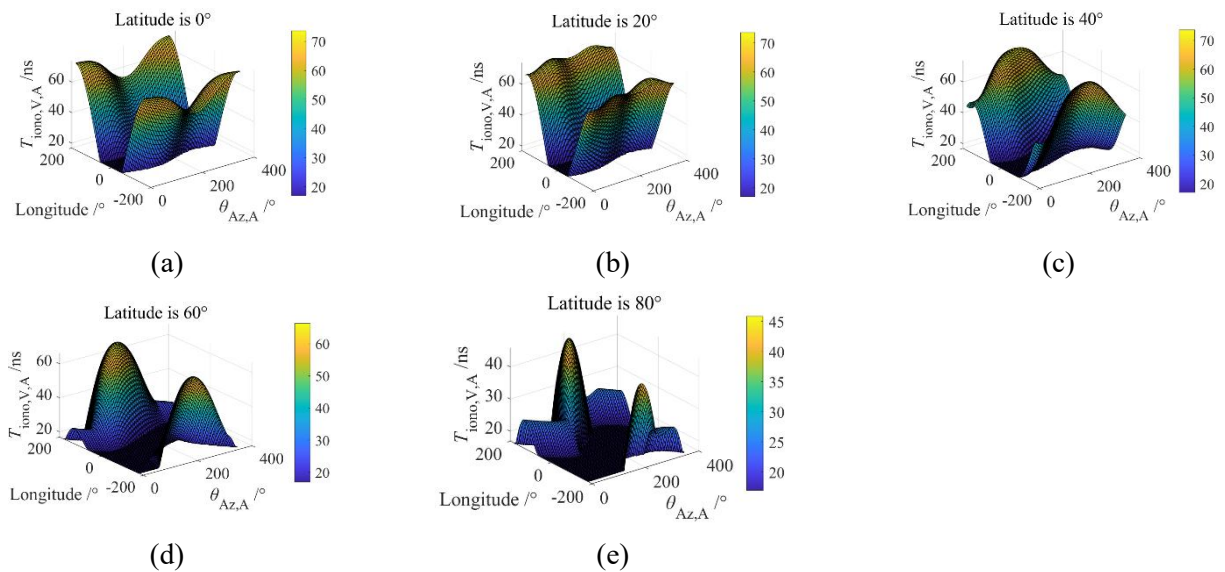


**Fig. 13.** The values of  $T_{iono,V,A}$  correspond to different values of the latitude, the longitude, and  $\theta_{Az,A}$ .

Fig. 13(a) to 14(e) illustrate that  $T_{\text{iono},V,A}$  decreases as the latitude of position A increases, suggesting that the maximum value of  $T_{\text{iono},V,A}$  may occur in low-latitude areas. Therefore, the latitude of position A is set to  $0^\circ$ . The rate of change of  $T_{\text{iono},V,A}$  with respect to  $\theta_{Az,A}$  is shown in Fig. 14. The corresponding values of  $\theta_{Az,A}$  and longitude when  $T_{\text{iono},V,A}$  reaches its maximum rate of change can be estimated as  $120^\circ$  and  $-90^\circ$ , respectively.

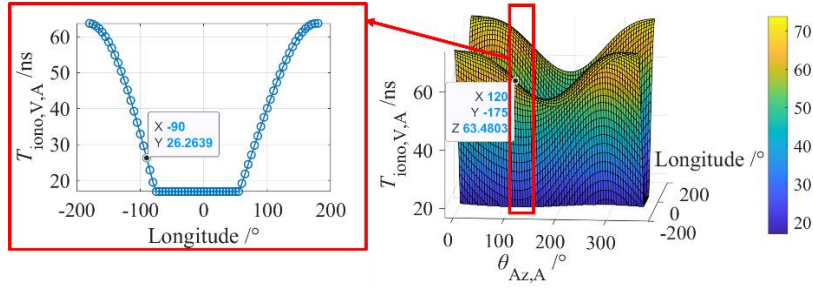


**Fig. 14.** The values of  $T_{\text{iono},V,T}$  correspond to different values of  $\theta_{Az,A}$  and the longitude when latitude is  $0^\circ$ .

When  $\|\mathbf{r}\|$  of 5000 m is on the E-N plane, the values of longitude and the latitude of position B are within the ranges  $[-89.9551^\circ, -90.0449^\circ]$  and  $[-0.0452^\circ, 0.0452^\circ]$ , respectively. In this case, the change of the latitude and the longitude are too small to traverse them to cover the position of the IPP. Therefore, the selection of  $t_A$  needs to be considered. Since the positive half cosine function is used to fit the vertical ionospheric delay except the nighttime period, the closer  $t_A$  approaches the endpoints of the nighttime interval, the greater the rate of change of the vertical ionospheric delay. The position error will make  $t_A$  change to  $t_B$ , which is the local time at IPP of position B. Therefore,  $t_A$  is selected close to the values of the endpoints (6 h and 22 h) but not exactly at them, to prevent  $T_{\text{iono},V,A}$  from becoming a constant when  $t_B$  is within the nighttime period.  $t_A$  is obtained by converting an observation epoch on September 5, 2023, which is about 21 h at position A.

When the position error is 5000 m, the corresponding values of  $\Delta T_{\text{iono}}$  to different values of longitude and latitude of position B are shown in Fig. 15. The absolute value of  $\Delta T_{\text{iono}}$ ,  $|T_{\text{iono}}|$ , is used to quantify the impact of positioning errors on ionospheric delay. The maximum  $|T_{\text{iono}}|$  is  $1.6 \times 10^{-1}$  ns, which corresponds to position B with geographic coordinates  $(0.0452^\circ\text{S}, 89.9551^\circ\text{W})$ . If  $\|\mathbf{r}\|$  decreases, that is, the difference of longitude and latitude between position B and position A decreases, then  $|T_{\text{iono}}|$  must be less than  $1.6 \times 10^{-1}$  ns.

The maximum value of  $|T_{\text{iono}}|$  is further analyzed with consideration of the azimuth. The maximum difference between the azimuth  $\theta_{Az,B}$  of position B and  $\theta_{Az,A}$  caused by  $\|\mathbf{r}\|$  of 5000 m is  $0.0266^\circ$ , of which calculation is shown in section 3.2. In Fig. 16, when  $\theta_{Az,B}$  is  $119.9870^\circ$ ,  $|T_{\text{iono}}|$  achieves its maximum  $1.6 \times 10^{-1}$  ns. Since  $|T_{\text{iono}}|$  analyzed above is based on position B  $(0.0452^\circ\text{S}, 89.9551^\circ\text{W})$ , that is,  $\|\mathbf{r}\|$  is 7070

m, the maximum value of  $|T_{\text{iono}}|$  when  $\|\mathbf{r}\|$  is 5000 m will be actually smaller than  $1.6 \times 10^{-1}$  ns. In other words, the ionospheric delay error caused by 5000 m position error is no more than  $1.6 \times 10^{-1}$  ns.

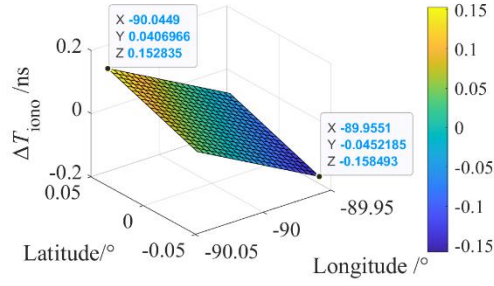


**Fig. 15.** The corresponding values of  $\Delta T_{\text{iono}}$  to different longitude and latitude values of position B when the position error is 5000 m.

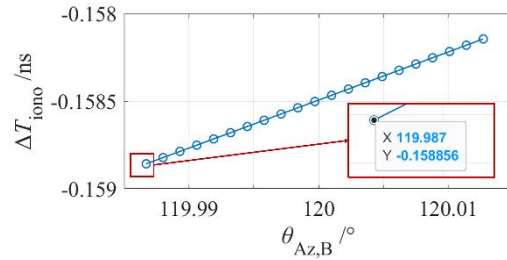


**Fig. 16.** The values of  $\Delta T_{\text{iono}}$  correspond to different azimuth values of position B.

When the projection of  $\mathbf{r}$  on the U-axis is not zero,  $\theta_{\text{El,B}}$  is the only variable in the calculation of  $\Delta T_{\text{iono}}$ .  $\theta_{\text{El,B}}$  varies from  $0^\circ$  to  $0.0133^\circ$ , and the corresponding values of  $\Delta T_{\text{iono}}$  are shown in Fig. 17. The maximum  $|T_{\text{iono}}|$  is  $1.3 \times 10^{-2}$  ns when  $\theta_{\text{El,B}}$  is  $0.0133^\circ$ . The maximum ionospheric delay error is estimated jointly by position error occurring in the N-E plane and the U-axis. In this way, the ionospheric delay error caused by 5000 m position error is no more than  $1.7 \times 10^{-1}$  ns, which is the sum of  $1.6 \times 10^{-1}$  ns and  $1.3 \times 10^{-2}$  ns.

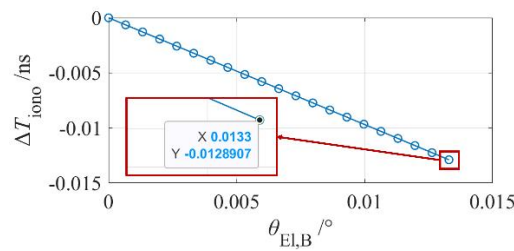


**Fig. 17.** The values of  $\Delta T_{\text{iono}}$  correspond to different values of  $\theta_{\text{El,B}}$ .

The same method is used for the analysis of 5 m position error and the ionospheric delay error is no more than  $1.7 \times 10^{-4}$  ns.

### 3.4. Combined impact on time transfer

The results from sections 3.1 to 3.3 indicate that the largest magnitude of the error caused by the position error occurs in the geometric distance delay. Therefore,  $\Delta T_{\text{geo}}$ ,  $\Delta T_{\text{tropo}}$ , and  $\Delta T_{\text{iono}}$  are compared in the scenario where  $\Delta T_{\text{geo}}$  is minimized, while  $\Delta T_{\text{tropo}}$  and  $\Delta T_{\text{iono}}$  are maximized. This scenario occurs when  $\theta_{\text{El,A}}$  is

0.0133° and both  $\Delta E$  and  $\Delta N$  are zero, as discussed in sections 3.2 and 3.3. When  $\|\mathbf{r}\|$  is 5000 m,  $\Delta T_{\text{geo}}$  is calculated to be 1533.8 ns by (5), which is 6 times larger than  $\Delta T_{\text{tropo}}$  of 230.6 ns and 8927 times larger than  $\Delta T_{\text{iono}}$  of  $1.7 \times 10^{-1}$  ns.

However, when  $\|\mathbf{r}\|$  is 5 m,  $\Delta T_{\text{geo}}$  of  $1.5 \times 10^{-6}$  ns calculated by (5) is smaller than  $\Delta T_{\text{tropo}}$  of 0.3 ns. Since the elevation of 0° is not common and it is the value of elevation mask angle set in R2CGGTTSv8.8 software, which is used for experiments, the analysis was conducted with  $\theta_{\text{El,A}}$  of 10°. The scenario where the absolute value of  $\Delta U$  is equal to  $\|\mathbf{r}\|$  and  $\theta_{\text{EA}}$  is 100° is shown in Fig. 18, making  $\Delta T_{\text{geo}}$  of 2.9 ns and  $\Delta T_{\text{tropo}}$  of  $5.1 \times 10^{-2}$  ns.  $\Delta T_{\text{geo}}$  will increase with the change of  $\theta_{\text{EA}}$  when  $\theta_{\text{EA}}$  is within the interval  $[0^\circ, 80^\circ] \cup [100^\circ, 180^\circ]$ . But  $\Delta T_{\text{tropo}}$  will not exceed  $5.1 \times 10^{-2}$  ns. These results show that, when the position error is 5 m,  $\Delta T_{\text{geo}}$  will be two orders of magnitude larger than  $\Delta T_{\text{tropo}}$  in about 89% of the cases ( $([0^\circ, 80^\circ] \cup [100^\circ, 180^\circ]) / 180^\circ \approx 0.89$ ). The ratio of 89% will increase as the position error increases.

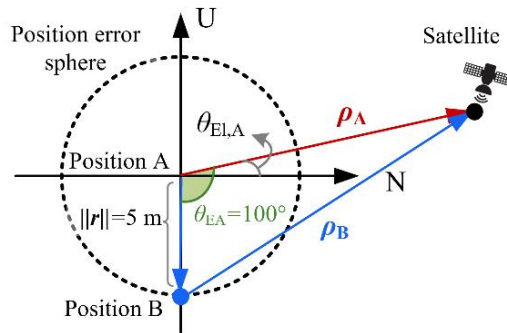


**Fig. 18.** The scenario where  $\theta_{\text{El,A}}$  is 10° and  $\|\mathbf{r}\|$  is 5 m.

$\Delta T_{\text{iono}}$  when  $\theta_{\text{El,A}}$  is 10° is no longer calculated since it is less than  $1.7 \times 10^{-4}$  ns, which is its maximum value and four orders of magnitude smaller than  $\Delta T_{\text{geo}}$  of 2.9 ns.

In summary, when  $\theta_{\text{EA}}$  is within the interval  $[0^\circ, 80^\circ] \cup [100^\circ, 180^\circ]$ ,  $\Delta T_{\text{geo}}$  is two orders of magnitude larger than  $\Delta T_{\text{tropo}}$  and four orders of magnitude larger than  $\Delta T_{\text{iono}}$ . Therefore, compared with the geometric distance delay error caused by the position error, the tropospheric delay error and the ionospheric delay error can be ignored. The time transfer error  $\Delta T_{\text{L-G}}$  can be estimated to  $\Delta T_{\text{geo}}$  and calculated by (16) and (17). The linear and cosine relationships between  $\|\mathbf{r}\|$ ,  $\theta_{\text{EA}}$ , and  $\Delta T_{\text{geo}}$  extend to  $\Delta T_{\text{L-G}}$ .

$$\begin{cases} \Delta T_{L-G} = k \|\mathbf{r}\| \\ k = -\frac{\|\mathbf{r}\| - \|\boldsymbol{\rho}_A\| \cos \theta_{EA}}{c\sqrt{\|\mathbf{r}\|^2 + \|\boldsymbol{\rho}_A\|^2 - 2\|\mathbf{r}\|\|\boldsymbol{\rho}_A\| \cos \theta_{EA}}} \end{cases} \quad (16)$$

$$\Delta T_{L-G} = A \cos \theta_{EA} \quad (17)$$

## 4. Experiments and results

In order to validate that the time transfer error is mainly caused by the geometric distance delay error and to assess the accuracy of (16) and (17), two experiments are designed. In experiment 1, comparisons will be made between the time transfer error, the tropospheric delay error, the ionospheric delay error, and the geometric distance delay error caused by different position errors. Experiment 2 will compare the theoretical time transfer error calculated based on (16) with the true time transfer error, and try to use the cosine function in the form of (17) to fit the true time transfer error when the position error is constant. The residuals are calculated to evaluate the performance of (16) and the cosine function fitting. Both experiments are based on real GNSS observation data.

### 4.1. Experiments setup

The GNSS time transfer receiver BJ02 referenced to TS(BJTU) which is an atomic time scale kept by our laboratory is used for obtaining GNSS data. Seven BDS and GPS satellites are selected, specifically satellites C05, C02, C28, C41, G32, G04, and G16. The BDS B1I data at 2:00:00 on September 5, 2023 and the GPS L1 C/A data at 13:00:00 on September 5, 2023 are used for analysis. The values of  $\theta_{El,A}$  for these satellites are shown in Table I. The higher elevation is about 20° or 30° higher than the lower one, to ensure an approximate uniform distribution of elevation ranging from 15° to 90°.

Table I.  $\theta_{El,A}$  of BDS and GPS Satellites

PRN	C05	C02	C28	C41	G32	G04	G16
$\theta_{El,A}/^\circ$	15.9	33.6	53.9	85.2	15.4	35.3	60.2

Both position A and position B are described in the local Cartesian coordinate system (E, N, U). Position A of BJ02 is calculated by the PPP technique.

In experiment 1, time transfer experiments with the real BDS and GPS signal and the Monte Carlo simulation experiments are designed.  $\Delta E$ ,  $\Delta N$  and  $\Delta U$ , ranging from -5000 m to 5000 m, are added to position A to generate position B. The software R2CGGTTSv8.8 is used to generate the 30-second files in Common GNSS Generic Time Transfer Standard (CGGTTS) format. The REFSYS values in these files with position A and position B are differentiated to represent  $\Delta T_{L-G}$ .  $\Delta T_{\text{tropo}}$  and  $\Delta T_{\text{iono}}$  are calculated based on MDTR and MDIO values in CGGTTS files, respectively.

In experiment 2, the cases with the coordinate error of -5000 m/5000 m are selected. The true time transfer error is  $\Delta T_{L-G}$  calculated in experiment 1, and the theoretical time transfer error is calculated by (16) or the fitted cosine function. The residual is represented by the absolute value of the difference between the theoretical and the true time transfer errors.

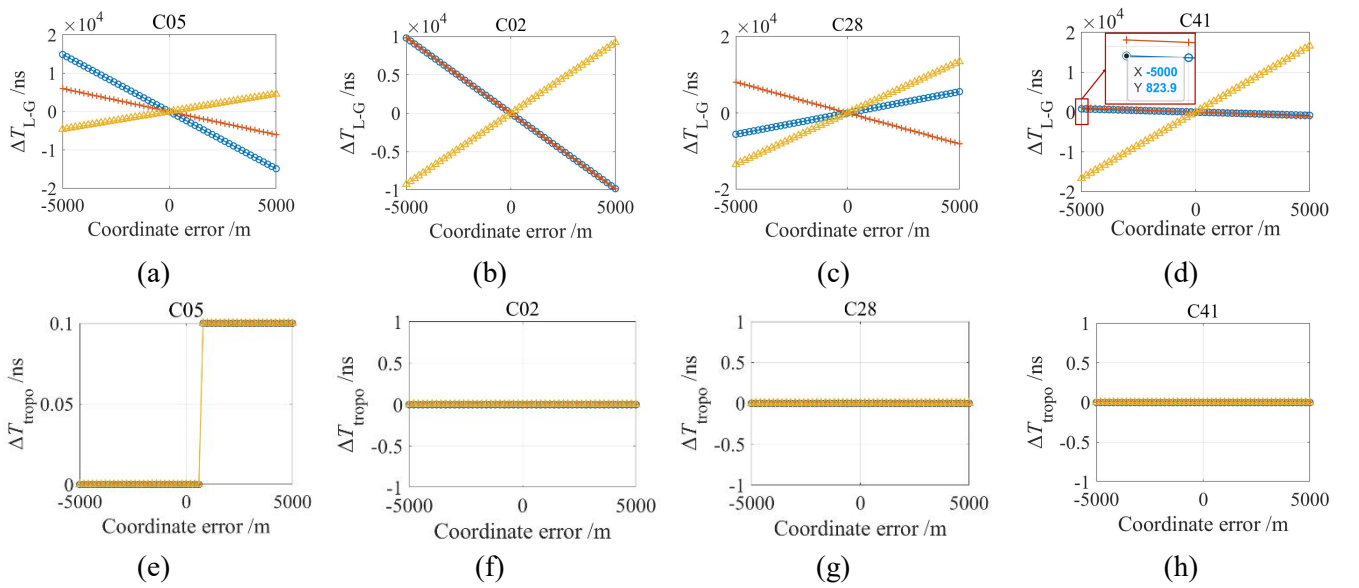
## 4.2. Results and discussion

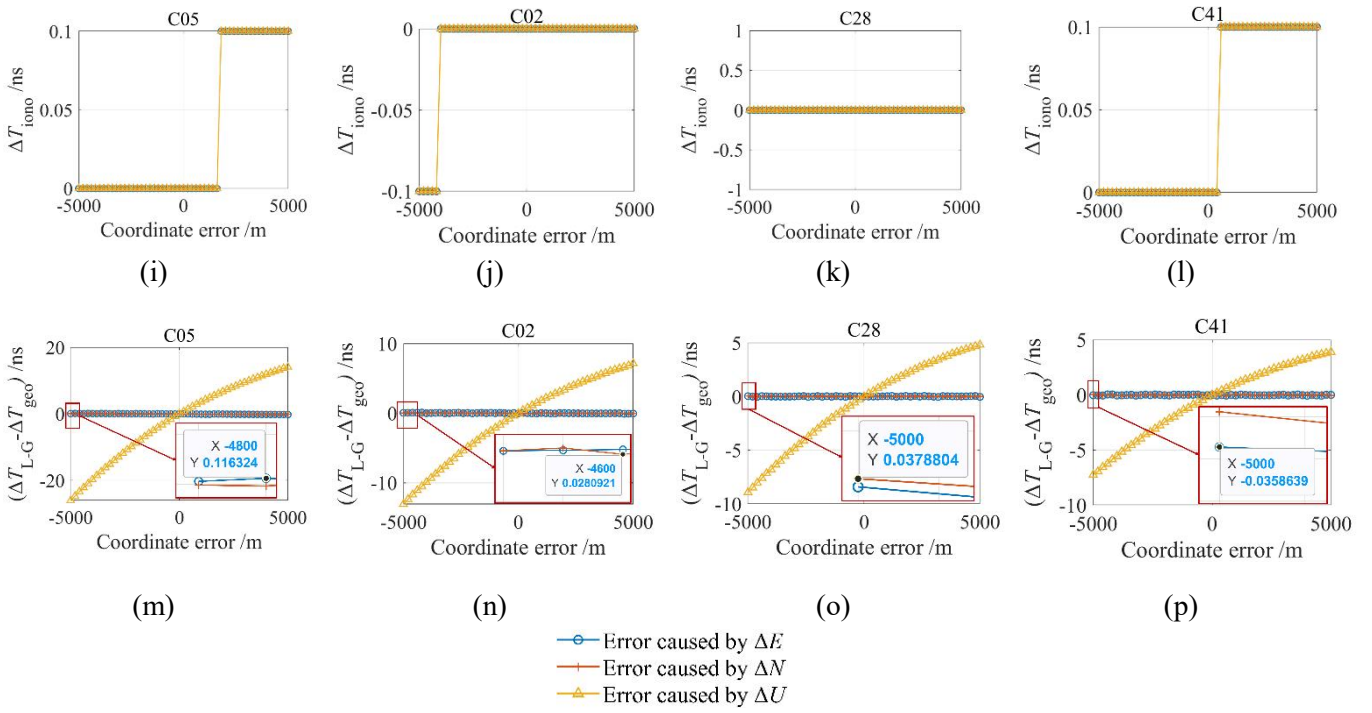
### 4.2.1 Experiment 1

$\Delta T_{L-G}$ ,  $\Delta T_{\text{tropo}}$ ,  $\Delta T_{\text{iono}}$  and  $\Delta T_{\text{geo}}$  of the BDS and the GPS satellites caused by  $\Delta E$ ,  $\Delta N$  and  $\Delta U$  are shown in Fig. 19(a) to 19(l) and Fig. 20(a) to 20(i). The higher  $\theta_{\text{El,A}}$  of the satellites is, the larger  $\Delta T_{L-G}$  caused by  $\Delta U$ , since  $\theta_{\text{EA}}$  is close to  $0^\circ$  or  $180^\circ$ . On the contrary, the effects of  $\Delta N$  and  $\Delta E$  on  $\Delta T_{L-G}$  reduce since  $\theta_{\text{EA}}$  approaches  $90^\circ$ . From the absolute value of  $\Delta T_{L-G}$  for the satellite C41,  $\Delta T_{L-G}$  caused by  $\Delta E$  is the smallest among all BDS and GPS cases, which is 823.9 ns when  $\Delta E$  is -5000 m. The jump values of 0.1 ns in  $\Delta T_{\text{tropo}}$  and  $\Delta T_{\text{iono}}$  are due to the 0.1 ns resolution of MDTR values and MDIO values. The absolute values of  $\Delta T_{\text{tropo}}$  and  $\Delta T_{\text{iono}}$  within the coordinate error of 5000 m do not exceed 0.1 ns, which are much smaller than  $\Delta T_{L-G}$  and can be negligible. The differences between  $\Delta T_{L-G}$  and  $\Delta T_{\text{geo}}$  of the BDS and the GPS satellites are shown in Fig. 19(m) to 19(p) and Fig. 20(j) to 20(l), which are much smaller than  $\Delta T_{L-G}$ , indicating that the geometric distance delay error is the main cause of the time transfer error. Since  $\Delta E$ ,  $\Delta N$  and  $\Delta U$  are added to position A respectively, the coordinate error can be treated as the position error. The linear relationship between  $\Delta T_{L-G}$  and the position error can be seen in each case, which is consistent with the theoretical analysis.

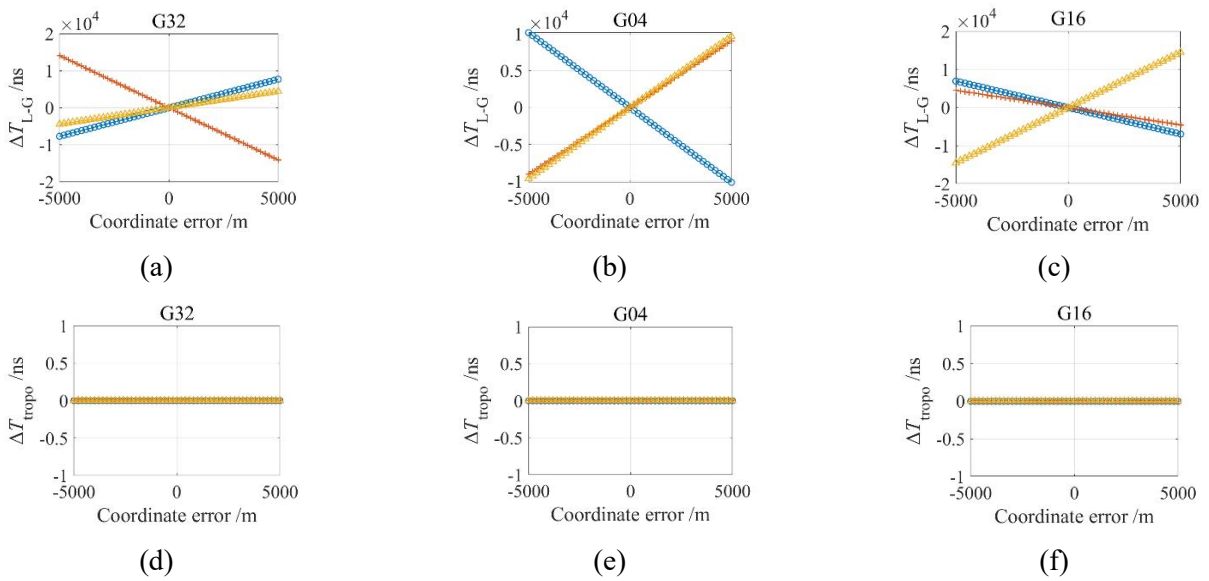
## 4.2.2 Experiment 2

$\theta_{\text{EA}}$  can be calculated based on the known coordinates of the satellites, position A, and position B. The true values of  $\Delta T_{L-G}$  are derived from the results of experiment 1 shown in Fig. 19 and Fig. 20. Table II and Table III show the theoretical  $\Delta T_{L-G}$  calculated by (16) and the true  $\Delta T_{L-G}$  at the coordinate error of -5000 m/5000 m of the BDS and the GPS satellites. The maximum residual is about 183 times smaller than the absolute value of the true  $\Delta T_{L-G}$ , which shows that the theoretical  $\Delta T_{L-G}$  and the true  $\Delta T_{L-G}$  are well consistent, indicating that the time transfer error caused by the position error can be estimated by (16) effectively. Table IV and Table V show the amplitude values of the fitted cosine functions and the residuals. The fitted cosine function, which takes the form of (17), is calculated based on  $\theta_{\text{EA}}$  and the true  $\Delta T_{L-G}$  of each satellite by ordinary least squares. The maximum residual 29.1 ns is about 158 times smaller than the absolute value of the true  $\Delta T_{L-G}$  4599.9 ns. It is demonstrated that the cosine function can be utilized to describe the relationship between  $\theta_{\text{EA}}$  and  $\Delta T_{L-G}$ .





**Fig. 19.** (a)~(d)  $\Delta T_{L-G}$  of the satellites C05, C02, C28 and C41. (e)~(h)  $\Delta T_{tropo}$  of the satellites C05, C02, C28 and C41. (i)~(l)  $\Delta T_{iono}$  of the satellites C05, C02, C28 and C41. (m)~(p) The differences between  $\Delta T_{L-G}$  and  $\Delta T_{geo}$  of the satellites C05, C02, C28 and C41.



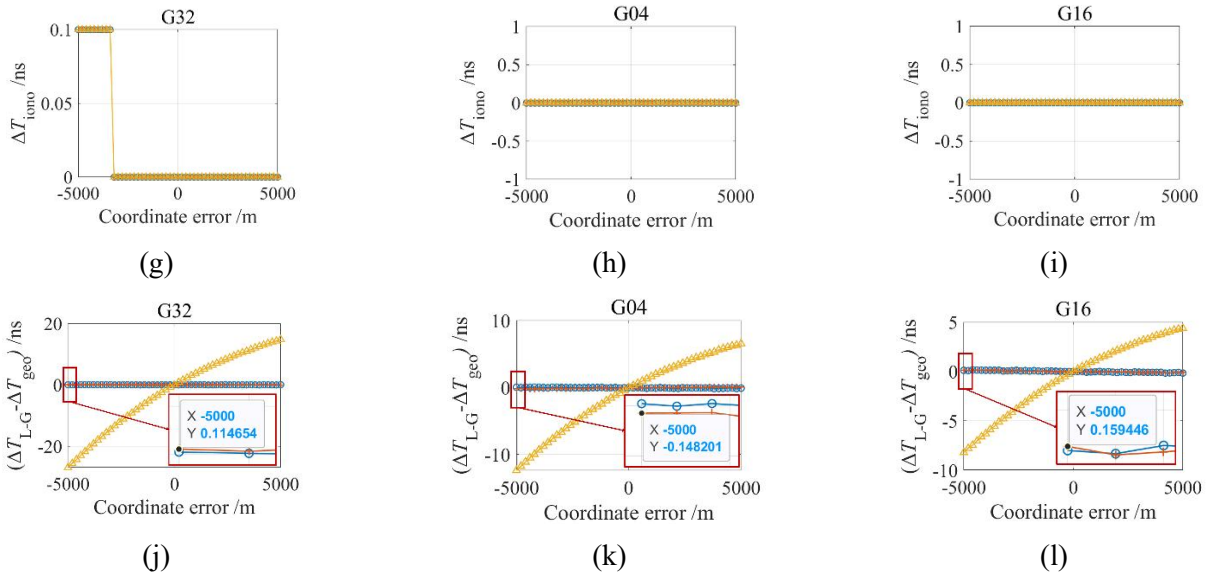


**Fig. 20.** (a)~(c)  $\Delta T_{L-G}$  of the satellites G32, G04 and G16. (d)~(f)  $\Delta T_{\text{tropo}}$  of the satellites G32, G04 and G16. (g)~(i)  $\Delta T_{\text{iono}}$  of the satellites G32, G04 and G16. (j)~(l) The differences between  $\Delta T_{L-G}$  and  $\Delta T_{\text{geo}}$  of the satellites G32, G04 and G16.

Table II. The theoretical and the true values of  $\Delta T_{L-G}$  for C05, C02, C28, and C41

PRN		Coordinate error /m					
		$\Delta E = -5000$	$\Delta E = 5000$	$\Delta N = -5000$	$\Delta N = 5000$	$\Delta U = -5000$	$\Delta U = 5000$
C05	$\theta_{EA} /^\circ$	26.9	153.1	68.9	111.1	105.9	74.1
	Theoretical $\Delta T_{L-G}$	14871.5	-14872.4	6004.5	-6008.1	-4574.8	4571.0
	/ns						
	True $\Delta T_{L-G}$ /ns	14871.8	-14872.4	6005.4	-6007.3	-4599.9	4586.0
	Residual /ns	0.3	0	0.9	0.8	25.1	15.0
C02	$\theta_{EA} /^\circ$	54.0	126.0	53.8	126.2	123.6	56.4
	Theoretical $\Delta T_{L-G}$	9807.6	-9810.5	9838.2	-9841.1	-9227.9	9224.9
	/ns						
	True $\Delta T_{L-G}$ /ns	9808.4	-9809.8	9839.0	-9840.4	-9240.2	9232.8
	Residual /ns	0.8	0.7	0.8	0.7	12.3	7.9
C28	$\theta_{EA} /^\circ$	109.6	70.4	61.0	119.0	143.9	36.1
	Theoretical $\Delta T_{L-G}$	-5586.0	5579.4	8089.2	-8094.9	-13474.0	13471.4

	$\theta_{EA}$ /°	87.2	92.8	86.1	93.9	175.2	4.8
C41	Theoretical $\Delta T_{L-G}$ /ns	822.0	-829.7	1116.4	-1124.1	-16620.1	16620.0
	True $\Delta T_{L-G}$ /ns	823.9	-827.8	1118.3	-1122.2	-16627.3	16623.9
	Residual /ns	1.9	1.9	1.9	1.9	7.2	3.9
	True $\Delta T_{L-G}$ /ns	-5584.3	5581.0	8090.7	-8093.5	-13482.3	13476.9
	Residual /ns	1.7	1.6	1.5	1.4	8.3	5.5

Table III. The theoretical and the true values of  $\Delta T_{L-G}$  for G32, G04 and G16

PRN		Coordinate error /m					
		$\Delta E = -5000$	$\Delta E = 5000$	$\Delta N = -5000$	$\Delta N = 5000$	$\Delta U = -5000$	$\Delta U = 5000$
G32	$\theta_{EA}$ /°	117.6	62.4	32.2	147.8	105.4	74.6
	Theoretical $\Delta T_{L-G}$ /ns	-7718.2	7712.8	14108.9	-14110.9	-4424.2	4417.7
	True $\Delta T_{L-G}$ /ns	-7716.8	7714.2	14109.5	-14110.4	-4449.5	4434.2
	Residual /ns	1.4	1.4	0.6	0.5	25.3	16.5
G04	$\theta_{EA}$ /°	52.5	127.5	122.9	57.1	125.3	54.7

	Theoretical $\Delta T_{L-G}$ /ns	10156.2	-10160.9	-9050.0	9044.7	-9652.0	9647.0
	True $\Delta T_{L-G}$ /ns	10157.4	-10159.8	-9048.8	9046.1	-9663.1	9654.8
	Residual /ns	1.2	1.1	1.2	1.4	11.1	7.8
	$\theta_{EA}$ /°	65.4	114.6	74.2	105.8	150.2	29.8
G16	Theoretical $\Delta T_{L-G}$ /ns	6931.7	-6938.4	4533.0	-4540.5	-14474.6	14472.6
	True $\Delta T_{L-G}$ /ns	6933.5	-6936.9	4535.0	-4538.7	-14482.3	14477.5
	Residual /ns	1.8	1.5	2.0	1.8	7.7	4.9

Table IV. The amplitude values and residuals for C05, C02, C28, and C41

PRN		Coordinate error /m					
		$\Delta E = -5000$	$\Delta E = 5000$	$\Delta N = -5000$	$\Delta N = 5000$	$\Delta U = -5000$	$\Delta U = 5000$
C05	Amplitude /ns	16684.2					
	Residual /ns	7.1	6.5	0.9	1.0	29.1	15.2
C02	Amplitude /ns	16679.3					
	Residual /ns	4.6	6.0	11.9	10.5	10.0	2.6
C28	Amplitude /ns	16680.3					
	Residual /ns	11.1	14.4	3.9	6.7	4.8	0.6
C41	Amplitude /ns	16683.7					
	Residual /ns	8.9	12.8	16.4	12.5	2.2	1.2

Table V. The amplitude values and residuals for G32, G04 and G16

PRN		Coordinate error /m					
		$\Delta E = -5000$	$\Delta E = 5000$	$\Delta N = -5000$	$\Delta N = 5000$	$\Delta U = -5000$	$\Delta U = 5000$
G32	Amplitude /ns	16673.8					
	Residual /ns	8.1	10.7	0.3	1.2	21.7	6.4
G04	Amplitude /ns	16687.5					
	Residual /ns	1.3	1.1	15.4	18.1	20.1	11.8
G16	Amplitude /ns	16680.1					
	Residual /ns	10.1	6.7	6.6	2.9	7.9	3.1

## 5. Conclusion

The error sources related to the position of the time transfer station in GNSS time transfer are analyzed individually to describe how they affect time transfer and quantify the impact of the position on GNSS time

transfer. The coordinate vectors of the receiver and the satellite are defined. The method for mapping them to GNSS time transfer is proposed. The error angle, defined based on the receiver and the satellite coordinate vector, is used to quantify the impact. The correction terms for the errors related to the receiver coordinates include the geometric distance delay, the ionospheric delay, and the tropospheric delay. The geometric distance delay error, which is two and four orders of magnitude larger than the tropospheric delay error and the ionospheric delay error separately, is the main cause of the time transfer error. An analytical expression describing the relationship between them is derived. For the identical value of position error, the time transfer error induced by the position error is different for different directions with respect to the true position. The time transfer error is maximized at 3.3 ns per meter of the position error when the error angle is  $0^\circ$  or  $180^\circ$ , and minimized when the error angle is  $90^\circ$ . However, maximum time transfer error is constrained to 3.3 ns with the position error of one meter. When the error angle is constant, there is an approximately linear relationship between the time transfer error and the position error. When the position error is constant, the time transfer error follows approximately a cosine relationship with the error angle.

## Acknowledgements

This work was supported by the National Natural Science Foundation of China with Grant No. 12473072, the TaiShan Industrial Experts Programme (tscx202408155), the Yantai Major Science&Technology Innovation and Development Project (2024ZDCX002) and the Open Foundation of The Center of National Railway Intelligent Transportation System Engineering and Technology (2023YJ360).

## References

- [1] White Paper: Application Technology of Next Generation Railway Carrying Network, China Railway Society, 2020.
- [2] P. Defraigne and G. Petit, "Time transfer to TAI using geodetic receivers," *Metrologia*, vol. 91, no. 4, 2003.
- [3] G. Petit and Z. Jiang, "Stability and accuracy of GPS P3 TAI time links," *2004 18th European Frequency and Time Forum (EFTF 2004)*, Guildford, 2004, pp. 287-291, doi: 10.1049/cp:20040870.
- [4] P. Defraigne and K. Verhasselt, "Multi-GNSS time transfer with CGGTTS-V2E," *2018 European Frequency and Time Forum (EFTF)*, Turin, Italy, 2018, pp. 270-275, doi: 10.1109/EFTF.2018.8409047.
- [5] G. Xu and Y. Xu, "GPS: Theory, algorithms and applications" 3rd ed, 2016.
- [6] J. Saastamoinen, "Atmospheric correction for the troposphere and stratosphere in radio ranging satellites," *The use of artificial satellites for geodesy*, vol.15, 1972.
- [7] H. S. Hopfield, "Tropospheric range error parameters: further studies", No. APL/JHU-CP-015, 1972.
- [8] A. E. Niell, "1996 Global mapping functions for the atmosphere delay at radio wavelengths," *Journal of geophysical research: solid earth*, vol.101, 1996.
- [9] J. Böhm, A. E. Niell, P. Tregoning and H. Schuh, "Global Mapping Function (GMF): A new empirical mapping function based on numerical weather model data," *Geophysical research letters*, vol. 33, 2006.
- [10] J. Böhm, B. Werl and H. Schuh, "Troposphere mapping functions for GPS and very long baseline interferometry from European Centre for Medium-Range Weather Forecasts operational analysis data," *Journal of geophysical research: solid earth*, vol. 111, 2006.
- [11] Q. Baire, P. Defraigne and E. Pottiaux, "Influence of troposphere in PPP time transfer," *2009 IEEE International Frequency Control Symposium Joint with the 22nd European Frequency and Time forum*, Besancon, France, 2009, pp. 1065-1068.
- [12] N. Wang, Y. Yuan, Z. Li and X. Huo, "Improvement of Klobuchar model for GNSS single-frequency ionospheric delay corrections," *Advances in Space Research*, vol. 57, 2016.

- [13] K.C.T. Swamy, A. D Sarma & A. Supraja Reddy, V. Satya Srinivas, P.V.D. Somasekhar Rao, "Modelling of GPS signal scintillations with polynomial coefficients over the Indian region", *Indian Journal of Radio & Space Physics (IJRSP) IJRSP*, vol. 42, no. 3, 2013.
- [14] K.C.T. Swamy, Devanaboyina, Venkata Ratnam, Nallagarla, Ramamurthy, Shaik, Towseef Ahmed and Turpati, Suman. "Correlation between rate of TEC index and positioning error during solar flares and geomagnetic storms using navigation with Indian constellation receiver measurements" *Journal of Applied Geodesy*, 2024.
- [15] S. Pireaux, P. Defraigne, L. Wauters, N. Bergeot, Q. "Baire and C. Bruyninx, Higher-order ionospheric effects in GPS time and frequency transfer". *GPS Solutions*, 14, 267-277.
- [16] K.C.T. Swamy, D. Venkata Ratnam, T. Suman and Towseef Ahmed Shaik, "Time-differenced double difference method for measurement of Navigation with Indian Constellation (NavIC) receiver differential phase bias", *Measurement*, vol. 207, pp. 112385, 2023.
- [17] G. Petit, J. Zhiheng, P. Urich, F. Taris, "Differential calibration of Ashtech Z12-T receivers for accurate time comparisons", *The 14th European Frequency and Time Forum (EFTF)*, Turin, Italy, May, 2000.
- [18] A. Proia, G. Cibiel, J. White, D. Wilson, K. Senior, "Absolute calibration of GNSS time transfer systems: NRL and CNES techniques comparison". *2011 Joint Conference of the IEEE International Frequency Control and the European Frequency and Time Forum (IFCS) Proceedings*, 2011, pp. 1-6.
- [19] J. Delporte, D. Valat, "CNES Accurate monitoring of GNSS time scales based on absolute calibration". *2022 Joint Conference of the European Frequency and Time Forum and IEEE International Frequency Control Symposium*, Paris, France, 24-28 Apr. 2022, pp. 1-5.
- [20] D. Valat, J. Delporte, "Absolute calibration of timing receiver chains at the nanosecond uncertainty level for GNSS time scales monitoring". *Metrologia*, 57, 2020.
- [21] E. Garbin, P. Defraigne, P. Krystek, R. Piriz, B. Bertrand and P. Waller. "Absolute calibration of GNSS timing stations and its applicability to real signals". *Metrologia*, 56, 2019.
- [22] I. Blinov, V. Fedoto, N. Koshelyaevsky. The First Absolute Delay Determination of GLONASS Time Receiver for TAI Time Transfer Link Calibration, *Proceedings of the 47th Annual Precise Time and Time Interval Systems and Applications Meeting*. Monterey, California, 25-28 Jan. 2016, pp. 223-230.
- [23] H. Chadsey, "How Bad Receiver Coordinates Can Affect GPS Timing," *Proceedings of the 27th Annual Precise Time and Time Interval Systems and Applications Meeting*, San Diego, California, United States of America, 1995, pp. 135-144.
- [24] Z. Ren, X. Huang, H. Gong, J. Peng and G. Sun, "BDS-3 RDSS two-way time transfer with asymmetric delay compensation model," *Measurement Science and Technology*, vol. 34, 2022.
- [25] P. Defraigne and G. Petit, "CGGTTS-Version 2E: an extended standard for GNSS Time Transfer," *Metrologia*, vol. 52, 2015.
- [26] BeiDou Navigation Satellite System Open Service Performance Standard (Version 3.0), BDS-OS-PS-3.0, China Satellite Navigation Office, 2016.